Spatial Temporal Analysis of Mesoscale Convective System to Asia-Australia Monsoon in East Java

Prasetyo Umar Firdianto[a,*], Bangun Muljo Sukojo[a], Achmad Zakir[b], Adi Mulsandi[c]

[a]Department of Geomatics Engineering, Institut Teknologi Sepuluh Nopember, Surabaya 60111, Indonesia

[b]Maritime Meteorological Station of Tanjung Perak, Indonesian Agency of Meteorology Climatology and Geophysics (BMKG), Kalimas Baru Street No. 97B, Surabaya 60165, Indonesia

[c]Indonesian State College of Meteorology Climatology and Geophysics (STMKG), Indonesian Agency of Meteorology Climatology and Geophysics (BMKG), Meteorologi Street No. 5, Tangerang Selatan 15221, Indonesia

*Corresponding author: prasetyo.firdianto@bmkg.go.id

Abstract. Indonesia maritime continent has the formation of clouds that can develop and evolution into MCSs (Mesoscale Convective System). Asian-Australian monsoon has an important influence in determining activities of MCSs. Research gap is analysis of relation between monsoon and MCSs in East Java where is greatly influenced by the monsoon. The data are weather satellite of Himawari, zonal wind and meridional wind ERA-Interim Model 850 mb. Determination of the MCSs follows the physical characteristics in the Maddox algorithm and the AUSMI index follows the Kajikawa algorithm. The method used is quantitative analysis of coefficient of correlation and determination, and qualitative in the form of descriptive analytic. It can be known that the Asian-Australian monsoon has weak influence on the MCSs in the East Java. AUSMI index has the same pattern and phase with frequency of MCSs on seasonal. The frequency of MCSs Meso-β is more dominant than Meso-α and the foremost life duration is 1-3 hours. The spatial distribution of MCSs Meso-β is more evenly distributed than MCSs Meso-α which only occur at certain times and point. The area that has a strong intensity of the occurrence of the most dominant MCSs is Southwestern of East Java.

Keywords: East Java; MCSs; Model; Monsoon; Satellite.

I. INTRODUCTION

The maritime continent of Indonesia is one of the tropical areas that has strong convective activity [1], [2], including the East Java region. This triggers the formation of convective clouds and can evolve and develop into a convective system in the form of MCSs (Mesoscale Convective System) [3]. MCSs are collections of clouds in certain areas (persistent areas) consisting of multi-cell thunderstorm clouds so that they can produce precipitation, have a length of more than 100 km and move in one direction [4], [5].

The Deep Convective process in tropical ocean areas [6], [7] consists of several Cumulonimbus clouds that have a base in the form of cirrus clouds with outflow in high layers [8]. When viewed from the number of cells, MCSs can be in the form of single cells, multicell, and supercells [9], [10], [11], [12]. Single cells have a life span of 20-30 minutes which can trigger bad weather, such as downbursts, hail, heavy rain, and tornadoes with weak intensity. While the combination of these single cells can form multiple cells that can trigger moderate hail and flash floods. Super cells are collections of storm clouds accompanied by updraft rotation that can result in strong downbursts, flash floods, and tornadoes.

The shape of MCSs in tropical regions can be circular and linear [13]. However, if MCSs are reviewed spatially, they can be classified into the Meso-β scale and the Meso-α scale. MCSs with a length of 25-250 km and a life duration of < 6 hours are included in the Meso-β scale. While MCSs with a length of 250-2500 km and a life duration of ≥ 6 hours are included in the Meso-α scale. The MCS identification process can use IR weather satellites [14], [15], [16], [17], namely by utilizing cloud top temperatures as observation objects.

Research of MCSs in Indonesia refers to the Maddox algorithm [13], namely with different locations, times, and methods analysis [18], [19], [20], [21], [22], [23]. However, some studies modify the physical characteristics of the algorithm to suit the conditions in the maritime continent [24], [25], [26], [27], [28], [29], [30]. Including MCSs in the form of QLCS (Quasi Linear Convective System). It can cause quite significant damage [31], [32], including strong winds and heavy rain. Research [26] states that MCSs with a circular shape in the form of MCSs that occurred in Jakarta on January 17, 2013 produced rainfall of 193 mm in 3 hours which is categorized as very

heavy rain according to BMKG (Meteorology, Climatology and Geophysics Agency). In addition, the MCSs phenomenon is influenced by monsoon activity [33], [34], [35], [36].

The maximum frequency of occurrence of Meso-α MCSs (Mesoscale Convective Complex/MCC) in the Indonesian region follows the seasonal radiation cycle and its movement follows the movement pattern of the Asian and Australian Monsoon systems [37]. MCSs precipitation is most prominent during Asia Monsoon and less dominant during Australia Monsoon [38], [39], [40]. That is December–January–February (DJF) season during Asia Monsoon and June–July–August (JJA) season during Australian Monsoon. Therefore, monsoon has an influence on the occurrence of MCSs.

The gap of research is analysis of relation between monsoon and mcs, including in East Java. Where the region is one of the regions that is greatly influenced by the monsoon phenomenon. That is the research problem that will be solved in this research.

Monsoon is a phenomenon that occurs in the wind system in tropical areas, where the wind direction moves in the opposite direction seasonally so that it affects the conditions of summer (summer rainfall) and winter (dry winter) [41], [42]. Monsoon activity results in differences in precipitation in a region and is in accordance with seasonal wind shifts [5].

Method to determine monsoon activity in the Asia-Australia region is to use the AUSMI (Australian Monsoon Index) index [43]. The AUSMI index is determined by calculating the average value of zonal winds at an altitude of 850 millibars in the area between 5–15° LS and 110–130° BT. The index can represent the variability of Monsoonal rainfall in parts of the Indonesian Maritime Continent and Northern Australia, including in the East Java region. Research of the AUSMI index is widely applied in Indonesia [44], [45], [46], [47]. The AUSMI index has very strong performance in the areas where the index is defined, including in East Java [48].

Therefore, the author conducted a study related to the influence of the Asian-Australian Monsoon on MCSs in the East Java region. It is hoped that with this study, it can determine the frequency of MCSs influenced by the Asian-Australian monsoon both spatially and temporally. Thus, the potential for disasters from the impacts caused can be reduced.

II. METHODOLOGY

2.1 Study Area Description

The research area domain used is the East Java region with an area coverage of 5.54° to 9.37° S and 110.83° to 114.72° E as shown in Figure 1.

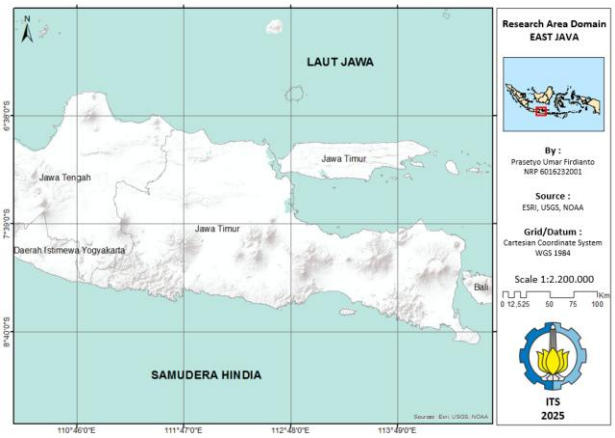

Figure 1. Research Area Domain

2.2 Materials

The data used in this study include Himawari Satellite data, ERA-Interim Model Reanalysis, and Rainfall. Himawari Satellite data on the infrared channel (IR1) in the period 2014-2018 (for 5 years) with portable gray map format (.pgm) and its calibration (.dat) obtained from Kochi University. The data can be accessed via http://weather.is.kochi-u.ac.jp/archive-e.html.

Zonal (u) and meridional (v) wind reanalysis data of the ERA-Interim model for the period 1988-2018 (for 30 years) in NetCDF (.nc) format obtained from ECMWF (European Centre for Medium-Range Weather Forecasts). The data can be accessed via https://apps-dev.ecmwf.int/datasets/data/interim-full-daily/levty%20pe=sfc/

Observation rainfall data of Tanjung Perak Maritime Meteorology Station (ID 96937) and East Java Climatology Station (ID 96943) monthly for 30 years (1989-2018). The data was obtained from BMKG.

2.3 Research Design

a) Identification of MCSs Using Himawari Satellite

IR satellite imagery data is selected for temperature (Temperature Black Body/TBB) that has a value of less than 221 K (-52° C) [13]. This temperature states the largest temperature limit of a cloud area in MCSs. In Meso-β MCSs, an area is selected that has a length of 25 km (area of 490.625 km^2) or close to 16 pixels, up to a length of 250 km (area of 4,9062.5 km^2) or close to 1622 pixels. Furthermore, in Meso-α MCSs for a length of 250 km (area of 49062.5 km^2) around 1622 pixels, up to a length of 2500 km (area of 4,906,250 km^2) around 162,152 pixels.

Find the center point of the selected area. The center point is the center of mass of the area that is connected to each other between pixels. The formula used to determine the center of mass is as shown by equations (1) and (2) [49].

$$X_0 = \frac{\sum_i^N X_i}{N} \quad \text{.....(1)}$$

$$Y_0 = \frac{\sum_i^N Y_i}{N} \quad \text{.....(2)}$$

X_i is *i*-th pixel at *X* axis. Y_i is *i*-th pixel at *Y* axis. X_0 is centre of X (Centroid *X*). Y_0 is centre of *Y* (Centroid *Y*). *N* is total area/total piksel. And *i* is *i*-th data.

The next step is to filter the shape of the MCSs convective cloud system with a quasi-circular shape. Therefore, an eccentricity value of ≥ 0.7 is used. The eccentricity value is a measure of the degree of ovality of a shape. In this case, the eccentricity method used is Least Square [50].

The eccentricity value (ε) is the ratio of the distance between the horizontal and vertical axis values. If the value is > 1, then the ratio is calculated the other way around so that the value is always ≤ 1. Where the value = 1 indicates a shape that is close to a circle and the value = 0 indicates an oval shape.

$$\alpha = \frac{(N\sum lat_i lon_i - \sum lat_i \sum lon_i)}{N\sum lat_i^2 - (\sum lat_i)^2} \quad \text{.....(3)}$$

$$\beta = Tan^{-1}\alpha \quad \text{.....(4)}$$

$$xx_i = lon_i \cos\beta + lat_i \sin\beta \quad \text{.....(5)}$$

$$yy_i = lon_i \sin\beta + lat_i \cos\beta \quad \text{.....(6)}$$

$$\varepsilon = \left|\frac{xx(max) - xx(min)}{yy(max) - yy(min)}\right| \quad \text{.....(7)}$$

$$\varepsilon = \left|\frac{yy(max) - yy(min)}{xx(max) - xx(min)}\right| \quad \text{.....(8)}$$

α is direction (regression coefficient). β is angle formed by a line with a horizontal axis. lat_i is latitude coordinate of *i*-th pixel. lon_i is longitude coordinate *i*-th pixel. *N* is total area or total pixel. xx_i is x axis coordinate of i-th point. yy_i is y axis coordinate of i-th point. *xx(max)* is maximum value of *x*. *xx(min)* is minimum value of *x*. *yy(max)* is maximum value of *y*. *yy(min)* is minimum value of *y*. ε is eccentricity value. *i* is *i*-th data.

The lifetime selection is carried out on the cloud cluster, namely 1-3 hours, 4-5 hours, and ≥ 6 hours. The duration applies to Meso-α and Meso-β MCSs. The lifetime is calculated based on the results of satellite observations of MCSs at consecutive times as shown in Figure 2.

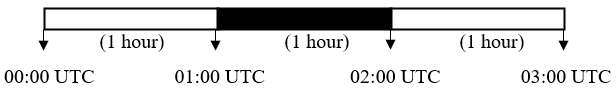

Figure 2. Simulation Determine MCSs Life Time

TABEL 1. MODIFICATION OF PHYSICAL CHARACTERISTIC OF MCSS

Parameter	Meso-α	Meso-β
TBB (Temperature of Black Body)	221 K (-52 °C)	
Length Size	250 – 2500 km	25 – 250 km
Eccentricity	≥ 0,7	
Life Time	1-3 hour , 4-5 hour, and ≥ 6 hour	

b) Identification of Asia-Australia Monsoon with AUSMI Indeks using ERA-Interim

Determination of the AUSMI index by calculating the average value of zonal winds at an altitude of 850 mb in the area between 5–15° LS and 110–130° BT [43] for 30 years (1998-2018). The determination is carried out seasonally (interannually), namely DJF (December, January, February), MAM (March, April, May), JJA (June, July, August), and SON (September, October, November).

c) Relation Analysis Technique of MCSs and Asia-Australia Monsoon

In analyzing the relationship between MCSs and Monsoon, several stages were carried out, including a comparison of AUSMI index data with rainfall observations from Meteorological Station of Tanjung Perak (Stamar Perak) and Climatological Station of Karangploso (Staklim Karangploso) in the form of a time scale graph. The frequency distribution of MCSs and AUSMI indexes seasonally for 5 years (2014-2018) is depicted in a graph against time. So that the variability between phenomena for Meso-α and Meso-β MCSs can be known. A review of the data center size in the boxplot diagram was carried out, including the average, quartiles 1-3, quartile range, maximum value and minimum value. Spatial mapping of MCSs distribution was carried out. In addition, interpolation was carried out using the krigging method to determine the intensity of the frequency of MCSs occurrence. So that areas with strong and weak intensity of MCSs can be identified. An analysis was carried out regarding the relationship between MCSs and the seasonal AUSMI index. This relationship is expressed by the correlation value as shown in equation 9. An analysis was carried out regarding the large role of monsoons on MCSs using the coefficient of determination in equation 10.

$$|r| = \frac{\sum_{i=1}^n (x_i - \overline{x})\cdot(y_i - \overline{y})}{\sqrt{\sum_{i=1}^n (x_i - \overline{x})^2 \cdot \sum_{i=1}^n (y_i - \overline{y})^2}} \quad \text{.....(9)}$$

$$KD = r^2 \quad \text{.....(10)}$$

$|r|$ is correlation value. *KD* is coefficient of determination. y_i is index value of AUSMI. x_i is total frequency of MCSs. $\overline{y_i}$ is mean indexs value of AUSMI. $\overline{x_i}$ is mean frequency of MCSs. *n* is total data.

TABEL 2. CORRELATION VALUE

Value	Relation
0.00 – 0.19	Very Weak
2.00 – 0.39	Weak
4.00 – 0.59	Medium
6.00 – 0.79	Strong
8.00 – 1.00	Very Strong

III. RESULT

3.1 Case Study of MCSs Meso-α

MCSs Meso-α with a length of 250-2500 km were observed on January 1, 2015 at 12.00-19.00 UTC (life time 8 hours) with physical characteristics as in Table 3 and spatial distribution of temperature of black body (IR1 channel) as in Figure 3.

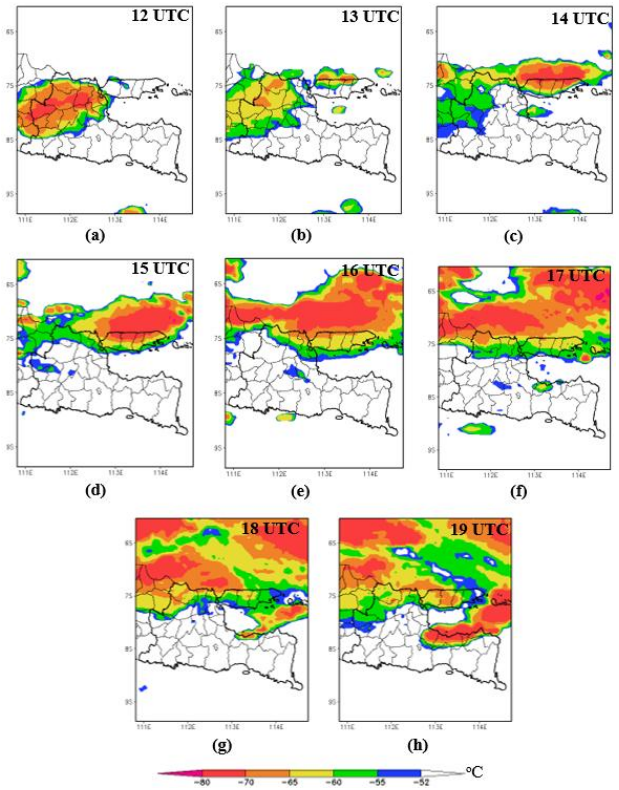

Figure 3. Case Study of MCSs Meso-α on 1 Januari 2015 (a) 12 UTC, (b) 13 UTC, (c) 14 UTC, (d) 15 UTC, (e) 16 UTC, (f) 17 UTC, (g) 18 UTC, dan (h) 19 UTC

TABEL 3. KARAKTERISTIK MCSS MESO-A TANGGAL 1 JANUARI 2015

Hour	ε	Pixel	*Long*	*Lat*
12	0.71	4796	112.83	-8.17
13	0.93	4953	112.79	-8.15
14	0.95	5007	112.65	-8.17
15	0.99	5285	112.39	-8.09
16	0.93	7192	112.75	-7.82
17	0.97	8507	112.5	-7.83
18	0.97	9319	112.26	-7.92
19	0.76	10252	112.25	-7.92

3.2 Case of MCSs Meso-β

Meso-β MCSs with a length of 25-250 km were observed on January 2, 2018 at 10.00-12.00 UTC (lifetime 3 hours) with physical characteristics as in Table 4 and spatial distribution of cloud top temperature (IR1 channel) as in Figure 4.

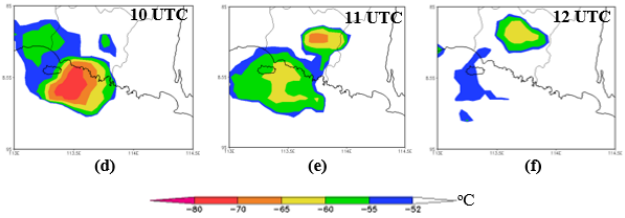

Figure 4. Case Study of MCSs Meso-β on 2 Januari 2015 jam (a) 10 UTC, (b) 11 UTC, dan (c) 12 UTC

TABEL 4. KARAKTERISTIK MCSS MESO-B TANGGAL 2 JANUARI 2018

Hour	ε	Pixel	*Long*	*Lat*
10	0.91	1412	112.27	-8.58
11	0.94	1164	111.78	-8.44
12	0.89	1009	111.33	-8.25

3.3 Comparison AUSMI Index and Rainfall Observation

Based on the results of processing 850 mb layer wind data from ECMWF in the AUSMI region (5–15° LS and 110–130° BT), the relationship with observed rainfall can be seen as shown in Figure 5.

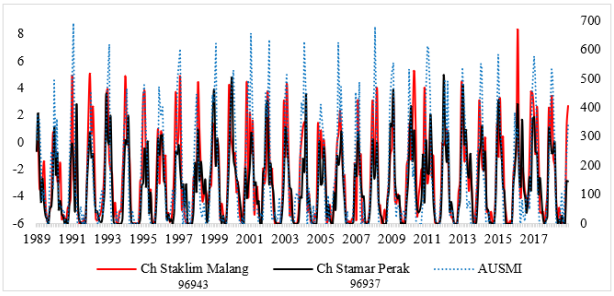

Figure 5. Comparison of AUSMI Index and Rainfall Observation in Jawa Timur Climatological Station (96943) and Tanjung Perak Meteorological Observation (96937)

From the graph, it can be seen that the AUSMI index has a strong relationship with the rainfall pattern in Staklim Malang and Stamar Perak. It is observed from the line pattern formed based on a time scale of 30 years. The correlation between the AUSMI index and rainfall in Staklim Malang shows a strong relationship, which is 0.68. In addition, it is followed by a correlation between the AUSMI index and rainfall in

Stamar Perak which is included in the strong category, which is 0.75. It can be concluded that the AUSMI index has a strong relation with rainfall in East Java.

3.4 Streamline of 850 mb at Asia-Australia Monsoon

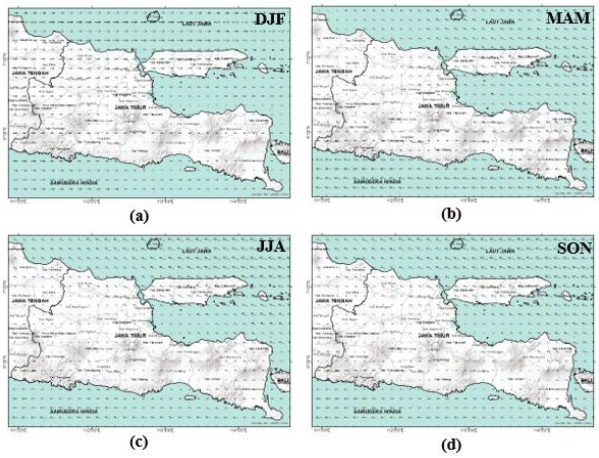

Figure 6. Spatial distribution of 850 mb layer winds seasonally a) DJF (December, January, February), b) MAM (March, April, May), c) JJA (June, July, August), d) SON (September, November, December).

From Figure 6, it can be seen that there are changes in wind direction and speed every month. In the December-Januari-February (DJF) month, the wind direction comes from the West which indicates the Asian (Western) monsoon and the flow of air masses from West to East. During the season transition, the wind direction in March-April-May (MAM) changes from East-Southeast which indicates the occurrence of the Australian (Eastern) monsoon. In Juni-July-August (JJA), the wind direction comes from the East-Southeast which indicates the Australian (Western) monsoon and the flow of air masses from West to East. In the next season transition, the wind direction in September-October-November (SON) tends to remain from the East-Southeast, indicating that the influence of the Australian monsoon is still quite strong. Therefore, in general it can be seen that the East Java region tends to be dominated by the Australian (Western) monsoon which is marked by the East wind blowing longer than the Westerly wind. The East wind blows in the months of MAM-SON. While the Westerly wind only blows in the month of DJF.

3.5 Temporal Fluctuation of MCSs

From Figure 7a, it can be seen that the highest number of MCSs events in the 2014-2018 period occurred in DJF 2014, which was 183 events. Graph 7a can be viewed from the changes in the number of MCSs events that occurred. In DJF-MAM 2014, there was a significant decrease in the number of events from 183 events to 55 events. In MAM-JJA 2014, the number of events tended to remain the same. In SON 2014 and DJF 2015, the number of events was quite significant, between 120-135 events. In DJF-MAM, there was a very significant decrease in the number of events from 120 to 23 events. In MAM-SON 2015, there was a gradual increase in the number of events. In DJF-MAM 2016, the number of events remained the same, namely 31 events. In MAM 2016-DJF 2017, the number of events increased gradually, from 31 events to 162 events. In MAM-SON 2017, the number of events tended to remain constant, between 97-101 events. In DJF-JJA, the number of events decreased gradually.

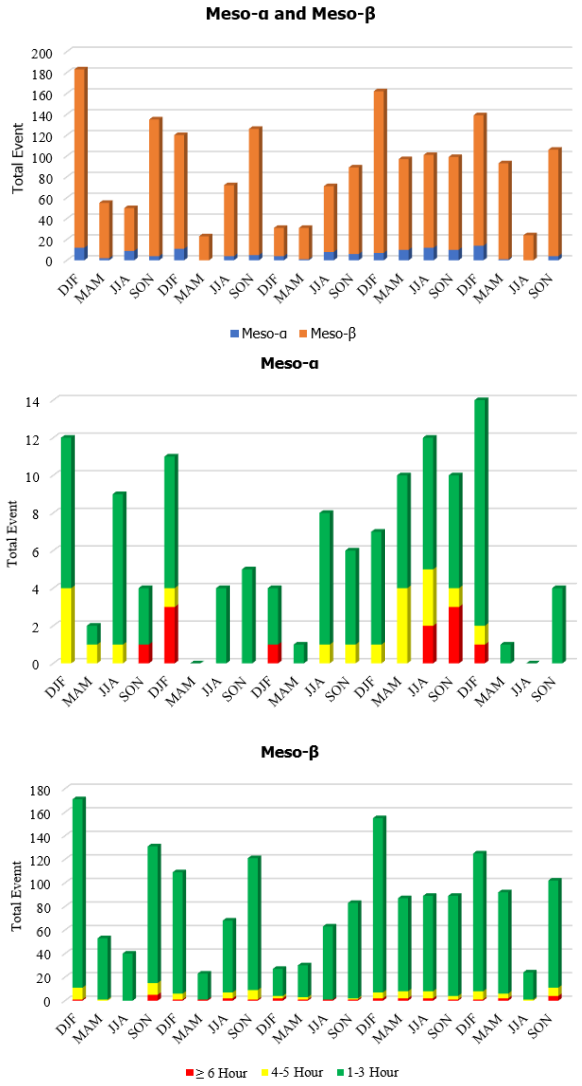

Figure 7. Temporal fluctuations of MCSs frequency per unit time a) based on Meso-α and Meso-β types, b) based on Meso-α lifetime, and c) based on Meso-β lifetime.

From Figure 7b, it can be seen that the highest number of Meso-α MCSs events in the 2014-2018 period occurred in DJF 2018, which was 14 events. The graph can be viewed from the changes in the number of MCSs events that occurred. In DJF-MAM 2014, there

was a significant decrease in the number of events from 12 events to 2 events. In MAM-JJA 2014, the number of events increased quite significantly. This has a similar pattern to the increase in SON 2014-DJF 2015. In DJF-MAM 2015, the number of events decreased very significantly, from 11 events to zero events. In MAM-SON 2015, the number of events increased gradually. In SON 2015-MAM 2016, the number of events increased gradually. In JJA 2016-DJF 2017, the number of events tended to remain the same. In MAM-JJA 2017, the number of events increased and was similar to SON 2017-DJF 2018. In DJF-JJA, the number of events decreased significantly, from 14 events to zero events.

From Figure 7c, it can be seen that the highest number of Meso-β MCSs events in the 2014-2018 period occurred in DJF 2014, which was 171 events. The graph can be viewed from the change in the number of MCSs events that occurred. In DJF-MAM 2014, there was a significant decrease in the number of events from 171 events to 53 events. In MAM-JJA 2014, the number of events tended to remain the same. In SON 2014 and DJF 2015, the number of events was quite significant, between 131-109 events. In DJF-MAM, there was a very significant decrease in the number of events from 109 to 23 events. In MAM-SON 2015, there was a gradual increase in the number of events. In DJF-MAM 2016, the number of events remained the same, at 27-30 events. In MAM 2016-DJF 2017, the number of events increased gradually, from 30 events to 155 events. In MAM-SON 2017, the number of events tended to remain the same, at 87-97 events. In DJF-JJA, the number of events decreased gradually.

3.6 *Frequency Percentage of MCSs*

From Figure 8a, we can see the comparison of Meso-α and Meso-β MCS percentages seasonally in the period 2014-2018 in the East Java region. It can be seen that the highest MCS frequency percentage is in the month of DJF, which is 35% of the total events or 639. The lowest MCS frequency percentage is in the month of MAM, which is 16% or 299 events. From Figure 8b, we can see the comparison of Meso-α MCS percentages. It can be seen that the highest MCS frequency percentage is in the month of DJF, which is 39% of the total events or 48. The lowest MCS frequency percentage is in the months of MAM and JJA, which is 14% or 11 events. From Figure 8c, we can see the comparison of Meso-β MCS percentages seasonally. It can be seen that the highest percentage of MCS frequency occurs in the month of DJF, which is 31% of the total occurrences or 587. The lowest percentage of MCS frequency occurs in the months of MAM and JJA, which is 17% or 285 occurrences.

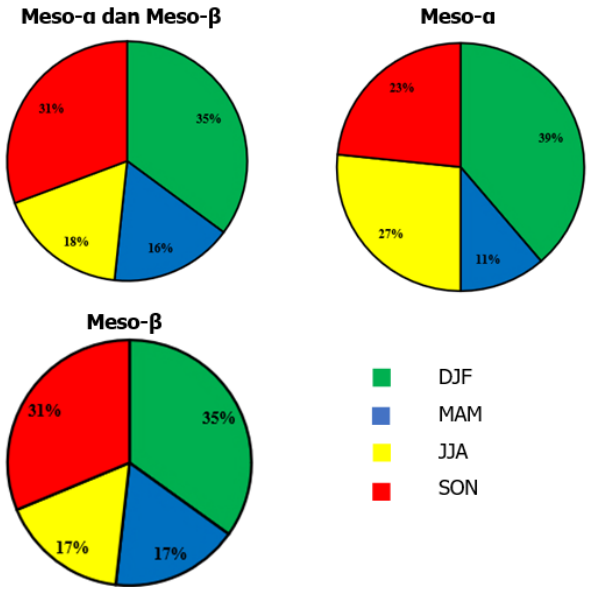

Figure 8. Percentage of MCSs frequency against time unit a) Meso-α and Meso-β, b) Meso-α, and c) Meso-β.

3.7 *Frequency Distribution of MCSs*

From Figure 9a, we can see the comparison of seasonal MCSs data distribution in the period 2014-2018 in the East Java region. The data distribution is shown in the range value, average (stated by the cross symbol), maximum (stated by the upper vertical line symbol), minimum (stated by the lower vertical line symbol), and quartile (1, 2, 3; stated by the circle symbol).

If the average value of all MCSs frequencies in the period 2014-2015 is carried out, an average value of 90-91 events can be obtained. Meanwhile, if viewed from the seasonal period, it can be seen that the highest average value occurs in the month of DJF. This value is 127 events. The lowest average value occurs in the month of MMA, which is 59-60 events. In addition, the level of seasonal MCSs frequency data density in this period can be seen. The data density is stated by the quartile range, which is the difference between the values of the third quartile and the first quartile. The smallest quartile range value occurred in the month of JJA, which was 27 events. So that the data in the month of SON has the highest distribution and data density level. While the largest quartile range value occurred in the month of MAM, which was 62 events. So that the data in the month of MAM has the lowest distribution and data density level.

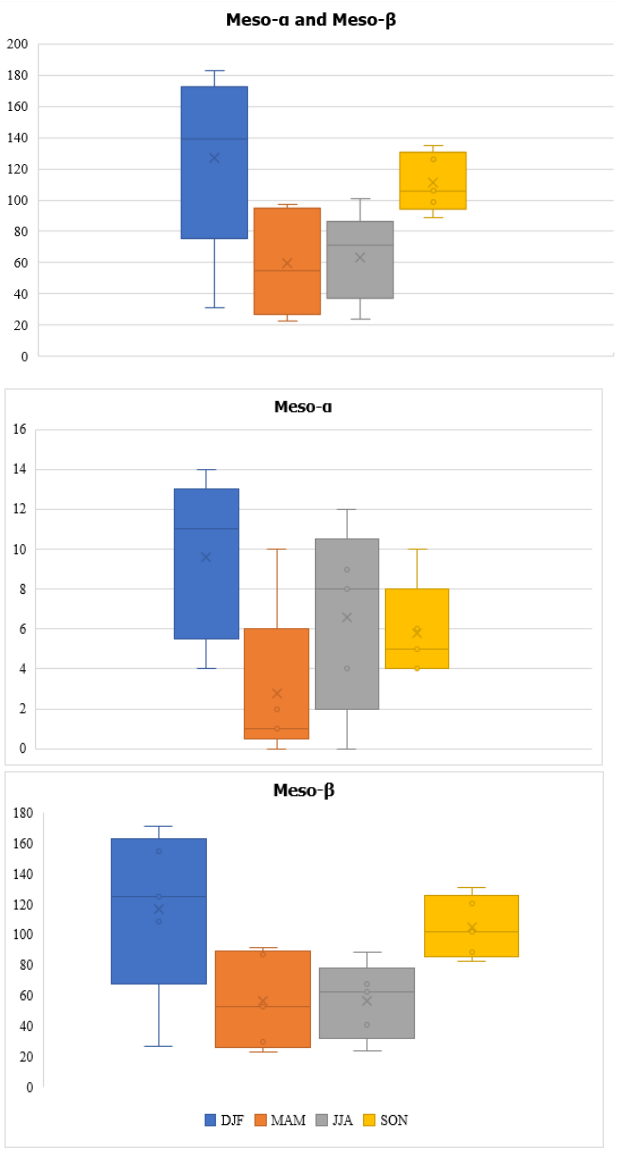

Figure 9. Distribution of MCSs frequency against time units a) Meso-α and Meso-β, b) Meso-α, and c) Meso-β.

From Figure 9b, we can see the comparison of the distribution of Meso-α MCSs data seasonally. If we average all MCSs frequencies in the 2014-2015 period, we can get an average value of 6-7 events per seasonal period. Meanwhile, if we look at the monthly average value, we can see that the highest average value occurs in the DJF month. This value is 9-10 events per seasonal period. The lowest average value occurs in the MMA month, which is 2-3 events per month. In addition, we can see the level of data density of monthly MCSs frequencies in that period. The smallest quartile range value occurs in the MAM month, which is 1 event. So that the data in the JJA month has the highest distribution and data density level. While the largest quartile range value occurs in the DJF and JJA months, which is 5 events. So that the data in the MAM month has the lowest distribution and data density level.

From Figure 9c, we can see the comparison of the distribution of MCSs data seasonally. If we average all MCSs frequencies in the period 2014-2015, we can get an average value of 90-91 events per seasonal period. Meanwhile, if we look at the monthly average value, we can see that the highest average value occurs in the month of DJF. This value is 127 events per seasonal period. The lowest average value occurs in the month of MMA, which is 59-60 events per month. In addition, we can see the level of data density of monthly MCSs frequencies in that period. The smallest quartile range value occurs in the month of JJA, which is 27 events. So that the data in the month of SON has the highest distribution and level of data density. While the largest quartile range value occurs in the month of MAM, which is 62 events. So that the data in the month of MAM has the lowest distribution and level of data density.

3.8 Spatial Distribution of MCSs

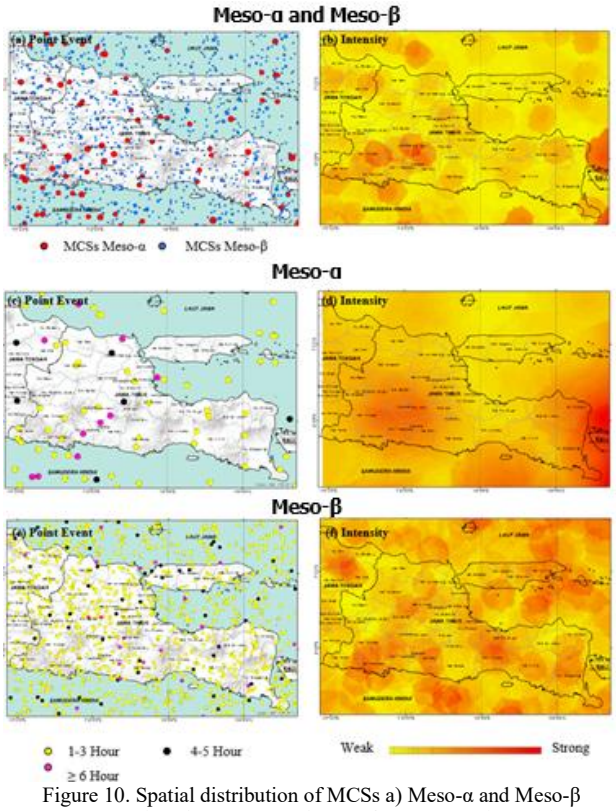

Figure 10. Spatial distribution of MCSs a) Meso-α and Meso-β occurrence points, b) Meso-α and Meso-β occurrence intensities, c) Meso-α occurrence points, d) Meso-α occurrence intensity, e) Meso-β occurrence points, and f) Meso-β occurrence intensity.

Based on the results of satellite data processing on the Meso-α and Meso-β MCSs phenomena in 2014-2018 in the East Java region, the spatial distribution can be seen as

shown in Figure 10. The MCSs occurrence point is shown in Figure 10a with the red circle legend being the Meso-α MCSs and the blue circle being the Meso-β MCSs. While the legends in Figures 10c and 10e state the duration of life of 1-3 hours, 4-5 hours, and ≥6 hours. The intensity of the MCSs occurrence is shown in Figures 10b, 10d, and 10f. The intensity of the occurrence is obtained from the results of interpolation using the krigging method so that the distribution of strong (stated in orange) and weak (stated in yellow) MCSs occurrences can be seen. In addition, the base map of the East Java region is equipped with topographic contours and boundary lines for each district or city.

From Figure 10a, it can be seen that the occurrence of Meso-β MCSs is more frequent and dominant than the occurrence of Meso-α MCSs. Meso-β MCSs occur evenly throughout almost all of East Java. While Meso-α MCSs only occur in certain areas. The frequency of Meso-α MCSs decreases around Madura Island and the North Java Sea. Meanwhile, if viewed from the intensity of the occurrence in Figure 10b, several areas have a strong frequency of Meso-α and Meso-β MCSs including Kediri Regency, Kediri City, Blitar City, Ponorogo Regency and part of Situbondo Regency.

From Figure 10c, it can be seen that the occurrence of Meso-α MCSs for a duration of 1-3 hours is more frequent and dominant than for a duration of 4-5 hours and ≥ 6 hours. Meso-α MCSs with a duration of 1-3 hours occur evenly throughout almost all of East Java, except on Madura Island. Meanwhile, Meso-α MCSs with a duration of 4-5 hours and ≥ 6 hours only occur in certain areas. If viewed from the intensity of the occurrence in Figure 10d, several areas have a strong frequency of Meso-α MCSs, including parts of Madiun, Nganjuk, Ponorogo, Trenggalek, Tulungagung, Kediri, Blitar, Bondowoso, Situbondo and Banyuwangi Regencies. While other areas have weak intensity.

From Figure 10e, it can be seen that the occurrence of Meso-β MCSs for a duration of 1-3 hours is more and dominates than for a duration of 4-5 hours and ≥ 6 hours. Meso-β MCSs with a duration of 1-3 hours occur evenly throughout almost all of East Java. Meanwhile, Meso-β MCSs with a duration of 4-5 hours and ≥ 6 hours only occur in certain areas. Meanwhile, if viewed from the intensity of the occurrence in Figure 10f, several areas have a strong frequency of Meso-β MCSs, including parts of Pacitan, Trenggalek, Ponorogo, Tulungagung, Kediri, Nganjuk, Blitar, Lumajang, Probolinggo, Banyuwangi, Pasuruan, Jombang, Lamongan, and Sumenep Regencies.

3.9 Seasonal Spatial Distribution of MCSs

From Figure 11, it can be seen that there are changes in the distribution of MCSs each season. In the month of DJF, the frequency of Meso-α and Meso-β MCSs tends to be high and is spread quite evenly in the East Java region. During this period, Meso-α MCSs only occur in certain areas, including Ponorogo, Kediri, Malang, Probolinggo, Bondowoso, and Banyuwangi Regencies. In addition, Meso-α MCSs occur in the waters of East Java in the Northwest, East, Southwest, Southeast, and Madura Strait. Meanwhile, in the waters of the Northeast, there is no such phenomenon. In the month of MAM, the frequency tends to decrease. It can be observed that there are quite significant changes in Meso-α MCSs. This incident occurred in the areas of Jombang, Tulungagung, and Pacitan Regencies. Meanwhile, Meso-β MCSs still have a fairly even distribution.

In the month of JJA, the frequency increased slightly. The areas where Meso-α MCSs occur include Tuban, Bojonegoro, Lamongan, Pacitan, Trenggalek, Tulungagung, Jombang, Pasuruan, and Luamajang Regencies. In the month of SON, the frequency of Meso-α and Meso-β experienced a significant increase so that the accumulation of events tended to be quite high. The areas where Meso-α MCSs occurred include Bojonegoro, Gresik, Sidoarjo, Kediri, Ponorogo, Blitar, Malang, and Jember. Meanwhile, Meso-β MCSs still have a fairly even distribution.

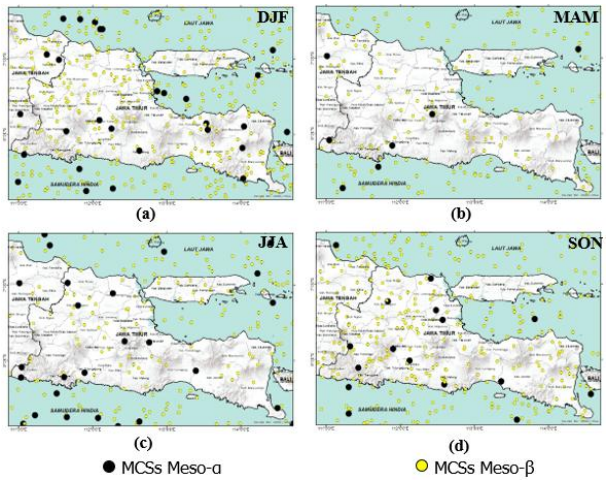

Figure 11. Spatial distribution of MCSs seasonally a) DJF months, b) MAM months, c) JJA months, and SON months.

Therefore, it can be generally known that during the Asian monsoon (DJF month) there is an increase in the frequency of MCSs in the North and Southeast parts of East Java compared to the Australian monsoon (JJA month). While during the monsoon transition in the SON month there is an increase in the frequency of MCSs in the Central, East, and Southeast parts of East Java compared to the monsoon transition in the MAM month.

3.10Period Analysis of MCSs Meso-α and MCSs Meso-β

Based on the MCS frequency data in Figure 7a, it can be seen that the frequency of Meso-β MCSs is very dominant compared to Meso-α MCSs. In addition, the number of Meso-α and Meso-β MCSs events has the most dominant

life phase of 1-3 hours. This is due to the less strong convective energy occurring in the East Java region. In general, this energy is only up to a certain magnitude so that dominant MCSs are formed only up to a scale of 25-250 km with a short life duration. However, when the energy is large, MCSs of 250-2500 km can be formed. The low convective energy is caused by the low supply of water vapor as the main ingredient in the formation of the Meso-scale convection system [51]. When the Asian monsoon is wet, water vapor tends to dominate in Sumatra and Kalimantan so that the water vapor content in the East Java region decreases. Meanwhile, water vapor from the Indian Ocean has difficulty reaching the East Java region because of the dry Australian monsoon.

3.11 Coefficient Correlation of Frequency MCSs and Monsoon

In Figure 12c, the change in the number of Meso-β MCSs and the AUSMI index is similar to the change in the number of MCSs as a whole. While for Meso-α MCSs, in general they still follow the AUSMI index phase but with a weaker relationship as shown in Figure 12b.

Statistically, the correlation between the frequency of MCSs and the seasonal AUSMI index is 0.473. The correlation between the frequency of Meso-β MCSs and the seasonal AUSMI index is 0.461. The correlation between the frequency of Meso-α MCSs and the seasonal AUSMI index is 0.398. The correlation values can be categorized as very moderate relationships. However, because the value is positive, it means that the frequency of MCSs has the same phase as the AUSMI index.

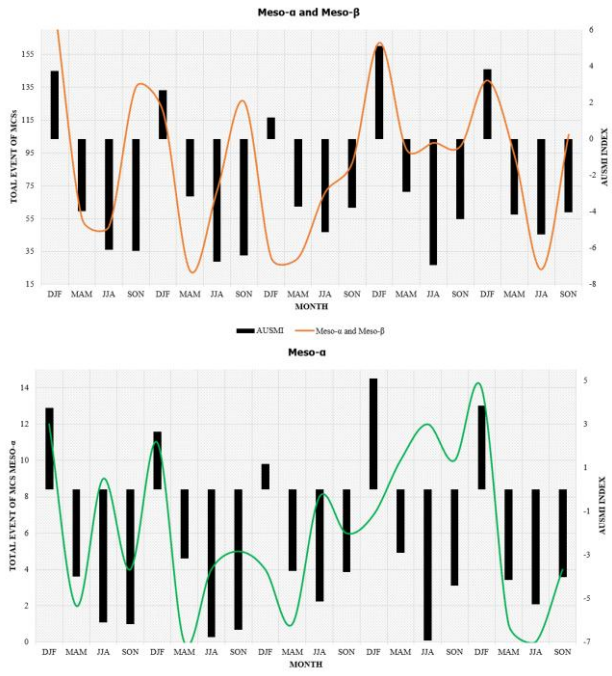

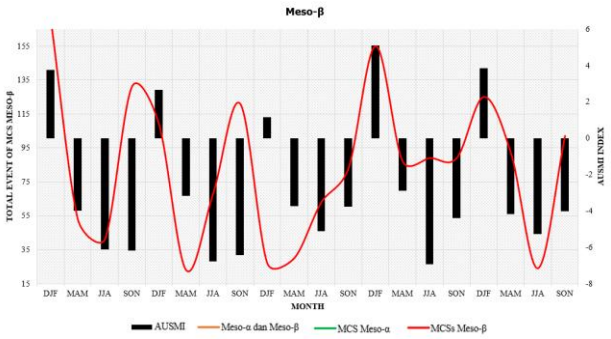

Figure 12. Comparison of MCSs Frequency and AUSMI Index a) Meso-α and Meso-β, b) Meso-α, and c) Meso-β.

3.12 Regression and Coefficient Determination of Frequency MCSs and Monsoon

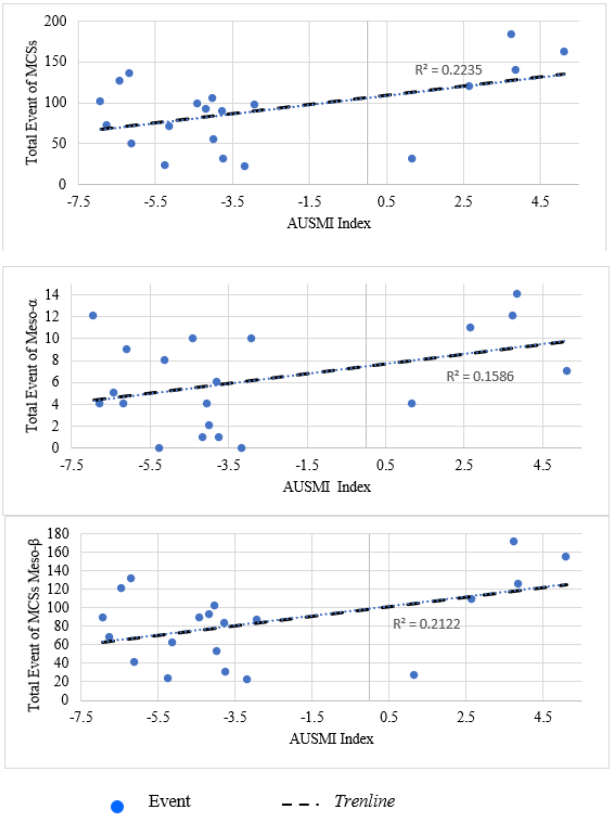

Figure 13. Comparison of MCSs frequency against AUSMI index seasonally a) Meso-α and Meso-β, b) Meso-α, and c) Meso-β.

In Figure 13, it can be generally seen that the greater the AUSMI index value, the greater the frequency of MCSs occurrence. This is indicated by the black trend line. A positive AUSMI index indicates the occurrence of the Asian monsoon and a negative AUSMI index indicates the occurrence of the Australian monsoon. So it can be concluded that the stronger the intensity of the Asian monsoon (positive and larger AUSMI index), the higher the frequency of MCSs that occur. The stronger the intensity of the Australian monsoon (negative and smaller

AUSMI index), the lower the frequency of MCSs that occur. The relationship between the frequency of MCSs and the AUSMI index can be shown by the gradient of the line (slope of the line) and the value of the coefficient of determination.

In addition, the determination value of Figure 13a (MCSs Meso-α and Meso-β) is 0.224. This means that the influence of the Asian-Australian monsoon on the frequency of MCSs seasonally is 22.4%. The determination value of Figure 13c (MCSs Meso-β) is 0.212. This means that the influence of the Asian-Australian monsoon on the frequency of MCSs Meso-β seasonally is 21.2%. The determination value of Figure 13b (MCSs Meso-α) is 0.159. This means that the influence of the Asian-Australian monsoon on the frequency of MCSs Meso-α seasonally is 15.9%.

3.13Spatial Analysis of MCSs on Monsoon Period

The spatial distribution of Meso-β MCSs is more even than Meso-α MCSs which only occur at certain times and locations. This is due to the convective process. Areas that have strong intensity of MCSs include Kediri Regency, Kediri City, Blitar City, Ponorogo Regency, and part of Situbondo Regency. Areas that have strong intensity of Meso-β MCSs include Pacitan, Trenggalek, Ponorogo, Tulungagung, Kediri, Nganjuk, Blitar, Lumajang, Probolinggo, Banyuwangi, Pasuruan, Jombang, Lamongan, and Sumenep Regencies. Areas that have strong intensity of Meso-α MCSs include Madiun, Nganjuk, Ponorogo, Trenggalek, Tulungagung, Kediri, Blitar, Bondowoso, Situbondo and Banyuwangi Regencies.

In general, it can be seen that the area that has the most dominant strong intensity of MCSs is Southwest East Java. This is due to the role of water vapor supply from the Indian Ocean that reaches the region so that MCSs are formed with high frequency. Warm oceans with large areas such as the Indian Ocean have a very strong diurnal cycle so that large convective systems are formed [51]. In addition, in this region it can be observed that most have a relatively high altitude than other regions (seen on the contour of the base map of the East Java region). Therefore, it is possible that the orographic process plays a role in increasing the convection process that occurs so that the power to form the mesoscale convective system is stronger.

During the Asian monsoon (DJF month) there is an increase in the frequency of MCSs in the northern and southeastern parts of East Java compared to the Australian monsoon (JJA month). Meanwhile, during the monsoon transition in the SON month, there is an increase in the frequency of MCSs in the Central, Eastern, and Southeastern parts of East Java compared to the monsoon transition in the MAM month.

IV. DISCUSSION

The case study on Januari 1-2, 2015 provide an overview of MCSs monitoring using the Himawari Satellite. MCSs is determined by physical characteristics as in Table 1. Through that method [37] produces hourly parameter values in the form of eccentricity, number of pixels, longitude, and latitude. From these parameters, the duration of life can be determined based on the hours of observation and the area of clouds based on the number of pixels. So it can be classified into MCSs Meso-α and Meso-β [13].

Comparison AUSMI index and rainfall observation means the index which have high relation with rainfall in East Java. This is in consistent with research [46], [48]. So that rainfall in East Java can be represented by the AUSMI index. Rainfall is related to the MCS which triggers extreme weather in area [23], [38].

Atmospheric conditions during Asia and Australia monsoon periods are represented by streamline 850 mb. Asia monsoon in December-Januari-February (DJF) period cause westerlies wind move from the Pacific and Asia Ocean to Australia Continent. Australia period causes reverse wind to Easterlies wind which have dry air mass in Juny-July-August (JJA). That is consistent with [41], [52], [53].

Temporal fluctuation of MCSs can be seen that the pattern of changes in the number of Meso-α and Meso-β MCSs events is fluctuating [37], [54], which applies when there is an increase or decrease. This means that there is a pattern of increase that is always followed by a pattern of decrease, and a pattern of decrease is always followed by a pattern of increase within a certain time. Frequency persentage of MCSs represent DJF season which have the most event than any other season. Because during its period the wet air mass from Asia Monsoon moves toward maritime continent, including East Java. In addition, frequency distribution of MCSs on its period have the most variability at presentation on figure 9.

Spatial Distribution of MCSs represent which strongest intensity area of cloud cluster occurrence is Southwest East Java. This is due to the role of water vapor supply from the Indian Ocean that reaches the area so that cloud clusters are formed with a high frequency. Warm oceans with large areas such as the Indian Ocean have a very strong diurnal cycle so that large convective systems are formed [55]. In addition, in this area it can be observed that most of them have a relatively high altitude than other areas. Therefore, it is possible that the orographic process plays a role in increasing the convection process [56], [57] that occurs so that the power to form the mesoscale convective system is getting stronger.

Coefficient Correlation of Frequency MCSs and Monsoon can be seen that the frequency of MCSs events follows the AUSMI index phase. When the West monsoon (AUSMI

index increases), there is an increase in the number of MCSs events and vice versa. However, in some periods, the time of change in the number of MCSs events tends to precede the time of change in the AUSMI index. Solar radiation plays an important role in the formation of MCSs. In the months of SON and DJF, MCSs have the highest frequency because at that time the sun is dominant in the East Java region. So that there is high convective activity. More analysis based on annual movement of the sun, maximum frequency occurs when the sun is in the East Java region between mid-October-November. The apparent annual circulation of the sun is explained by [2], [52]. In mid-October, the sun has maximum radiation in the East Java region. Because the ocean as the main source of water vapor supply has latent heat, the maximum convection process occurs in November. Therefore, in general, the maximum frequency of cloud clusters occurs in November and December.

Regression and Coefficient Determination of Frequency MCSs and Monsoon can be seen that the Asian-Australian monsoon has a low contribution to the occurrence of MCSs. This can be observed in the correlation coefficient and determination coefficient which have small values. There are other factors with a greater role in the formation of the MCSs phenomenon. This complements the research [37] which states that there is a role for the monsoon in the formation of MCSs. In addition, the influence of monsoon (AUSMI index) on the MCSs seasonally is more influential than monthly. This is observed from the gradient of the line and the coefficient of determination which have higher values during the season than during the month. Therefore, that due to the presence of other phenomena with larger oscillation periods that affect the frequency of cloud clusters, including ENSO (El-Nino Southern Oscillation), PDO (Pacific Decadal Oscillation), QBO (Quasi Biennial Oscillation), and others. Meanwhile, the intensity of the monsoon greatly affects the frequency of MCSs Meso-α. When the intensity of the monsoon is stronger, the number of cloud cluster events tends to be higher. When the intensity of the monsoon is weaker, the number of cloud cluster events tends to be lower.

From all of the method and result of the research have some limitations of the study. Spatial of MCSs is classified based on [13], [15], that is 25-250 km for Meso-β and 250-2500 km for Meso-α. Therefore physical characteristic of MCSs based on [13]. Analysis of Asia and Australia Monsoon based on the AUSMI index because it has strong correlation with rainfall in East Java [27]. In addition, East Java is an area included in the domain of determining the AUSMI index [43]. Data period is 5 years because it is considered to represent the characteristics of regional parameters and the phenomena that occur. The period is a seasonal (interannual) which in this study began in 2013 (December), 2014-2017 (January-December), and 2018 (January-November).

V. CONCLUSION

The Asian-Australian monsoon has a less significant influence on the MCSs in the East Java region. This is indicated by the weak correlation coefficient value and the small determination coefficient value. However, AUSMI index has the same pattern and phase as MCSs frequency seasonally. Contribution of the Asian-Australian monsoon on the frequency of MCSs Meso-α and Meso-β 22.4%, Meso-β 21.2%, and Meso-α 15.9%.

The frequency of MCSs events of Meso-β is very dominant compared to MCSs of Meso-α. In addition, the frequency of MCSs events of Meso-α and Meso-β have the most dominant life phase of 1-3 hours. On seasonally, MCSs events have a maximum frequency in DJF period (Asian monsoon). The intensity of the monsoon has quite an influence on the frequency of MCSs that occur. When the intensity of the monsoon is stronger, the number of MCS events tends to be higher. When the monsoon intensity is getting weaker, the number of MCSs events tends to be lower.

The spatial distribution of MCSs Meso-β is more even than MCSs Meso-α which only occur at certain times and locations. The area with the strongest intensity of MCSs is the Southwestern of East Java. In addition, it can be seen that during the Asian monsoon (DJF period) there is an increase in the frequency of MCSs in the North and Southeast parts of East Java compared to the Australian monsoon (JJA month). Meanwhile, during the monsoon transition in the SON period, there is an increase in the frequency of MCSs in the Central, East, and Southeast parts of East Java compared to the monsoon transition in the MAM month.

ACKNOWLEDGEMENT

The author would like to thank LPDP (Education Fund Management Institute) for the support of educational scholarships for the author and research funds that have been provided so that this research can be carried out properly.

REFERENCES

[1] D. Argüeso, R. Romero, and V. Homar, “Precipitation features of the maritime continent in parameterized and explicit convection models,” *J. Clim.*, vol. 33, no. 6, pp. 2449–2466, 2020, doi: 10.1175/JCLI-D-19-0416.1.

[2] B. Tjasyono, *Karakteristik dan Sirkulasi Atmosfer*, vol. I. Jakarta: Badan Meteorologi Klimatologi dan Geofisika, 2009.

[3] M. Muetzelfeldt, R. Plant, and H. Christensen,

"Environmental Conditions Affecting Global Mesoscale Convective System Occurrence," no. February, pp. 391–407, 2025, doi: 10.1175/JAS-D-24-0058.1.

[4] W. R. Cotton and R. A. Anthes, "Chapter 10 Mesoscale Convective Systems," *Int. Geophys.*, vol. 44, no. C, pp. 593–713, Jan. 1992, doi: 10.1016/S0074-6142(08)60549-5.

[5] A. Laing and J.-L. Evans, "Introduction to Tropical Meteorology," *COMET Progr.*, no. March, p. 2016, 2016, [Online]. Available: http://www.meted.ucar.edu/tropical/textbook_2nd_edition/

[6] M. R. Igel and S. C. van den Heever, "Tropical, oceanic, deep convective cloud morphology as observed by CloudSat," *Atmos. Chem. Phys. Discuss.*, vol. 15, pp. 15977–16017, 2015, doi: 10.5194/acpd-15-15977-2015.

[7] S. Samuel, N. Mathew, and V. Sathiyamoorthy, "Association of the occurrence of deep convective cloud cores with sea surface temperatures over the equatorial Indian and the western Pacific oceans," *Atmos. Res.*, vol. 269, p. 106034, May 2022, doi: 10.1016/J.ATMOSRES.2022.106034.

[8] J. Strandgren, L. Bugliaro, F. Sehnke, and L. Schröder, "Cirrus cloud retrieval with MSG/SEVIRI using artificial neural networks," *Atmos. Meas. Tech.*, vol. 10, no. 9, pp. 3547–3573, 2017, doi: 10.5194/amt-10-3547-2017.

[9] J. M. L. Dahl, "Supercells - Their Dynamics and Prediction," p. 122, 2006.

[10] Kyaw Than Oo, "Review of the History of Mesoscale Convective System Forecasts on Aviation," *J. Airl. Oper. Aviat. Manag.*, vol. 2, no. 1, pp. 68–85, 2023, doi: 10.56801/jaoam.v2i1.4.

[11] P. Markowski and Y. Richardson, "Mesoscale Meteorology in Midlatitudes," *Mesoscale Meteorol. Midlatitudes*, pp. 1–407, 2010, doi: 10.1002/9780470682104.

[12] F. Wan, Z. Liu, and H. Pang, "Supercell Storm and Extreme Wind in a Linear Mesoscale Convective System," in *2021 IEEE 23rd Int Conf on High Performance Computing & Communications; 7th Int Conf on Data Science & Systems; 19th Int Conf on Smart City; 7th Int Conf on Dependability in Sensor, Cloud & Big Data Systems & Application (HPCC/DSS/SmartCity/DependSys)*, 2021, pp. 2264–2269. doi: 10.1109/HPCC-DSS-SmartCity-DependSys53884.2021.00339.

[13] R. A. Maddox, "Meoscale Convective Complexes," *Bull. Am. Meteorol. Soc.*, vol. 61, no. 11, pp. 1374–1387, 1980, doi: 10.1175/1520-0477(1980)061<1374:mcc>2.0.co;2.

[14] Z. Feng *et al.*, "A Global High-Resolution Mesoscale Convective System Database Using Satellite-Derived Cloud Tops, Surface Precipitation, and Tracking," *J. Geophys. Res. Atmos.*, vol. 126, no. 8, pp. 1–29, 2021, doi: 10.1029/2020JD034202.

[15] I. L. Jirak, W. R. Cotton, and R. L. McAnelly, "Satellite and radar survey of mesoscale convective system development," *Mon. Weather Rev.*, vol. 131, no. 10, pp. 2428–2449, 2003, doi: 10.1175/1520-0493(2003)131<2428:SARSOM>2.0.CO;2.

[16] K. Whitehall *et al.*, "Exploring a graph theory based algorithm for automated identification and characterization of large mesoscale convective systems in satellite datasets," *Earth Sci. Informatics*, vol. 8, no. 3, pp. 663–675, 2015, doi: 10.1007/s12145-014-0181-3.

[17] R. Xiang *et al.*, "Monitoring Mesoscale Convective System Using Swin-Unet Network Based on Daytime True Color Composite Images of Fengyun-4B," *Remote Sens.*, vol. 15, no. 23, 2023, doi: 10.3390/rs15235572.

[18] R. W. S. Saragih, "Identifikasi Karakteristik Mesoscale Convective Complex (MCC) di Wilayah Papua dan Sekitarnya," *J. Fis.*, vol. 12, no. 2, pp. 42–54, 2022, doi: 10.15294/jf.v12i2.39190.

[19] D. Septiadi and Y. S Nugraha, "Dampaknya Terhadap Curah Hujan Di Benua Maritim Indonesia (Bmi) Sepanjang Tahun 2018 Identification of Mesoscale Convective Complex (Mcc) and Its Impact Over the Indonesia Maritime Continent During 2018," no. Mcc, pp. 73–80, 2020.

[20] L. Febrizky, M. Fadli, and W. Wiliam, "Identifikasi Mesoscale Convective Complex (Mcc) Berbasis Data Satelit Himawari-8 Di Pulau Papua Dan Sekitarnya Desember 2021-November 2022," *Opt. J. Pendidik. Fis.*, vol. 7, no. 2, pp. 294–305, 2023, doi: 10.37478/optika.v7i2.3132.

[21] R. Nurpambudi, H. Ismanto, S. Tinggi, M. Klimatologi, and B. Meteorologi, "Simulasi Mesoscale Convective System Menggunakan Model Wrf-Arw Di Makassar," pp. 1–11, 2015.

[22] E. Diniyati and Y. Donni Haryanto, "Identifikasi Fenomena Mesoscale Convective System (MCC) di Selat Karimata," *KELUWIH J. Sains dan Teknol.*, vol. 2, no. 2, pp. 103–111, 2021, doi: 10.24123/saintek.v2i2.4541.

[23] A. F. Rais, R. Yunita, and T. S. Hananto, "Pengaruh Mesoscale Convective System terhadap Hujan Ekstrem Pesisir Barat Sumatra," *Maj. Geogr. Indones.*, vol. 35, no. 1, p. 9, 2021, doi: 10.22146/mgi.60598.

[24] N. S. Putri, T. Hayasaka, and K. D. Whitehall, "The properties of mesoscale convective systems in Indonesia detected using the grab 'em tag 'em graph 'em (GTG) algorithm," *J. Meteorol. Soc. Japan*, vol. 95, no. 6, pp. 391–409, 2017, doi: 10.2151/jmsj.2017-

026.

[25] Y. Norman and N. J. Trilaksono, "Investigation of Mesoscale Convective Systems over Indonesian Maritime Continent using Geostationary Meteorological Satellite," *J. Phys. Conf. Ser.*, vol. 1204, no. 1, 2019, doi: 10.1088/1742-6596/1204/1/012124.

[26] D. E. Nuryanto, H. Pawitan, R. Hidayat, and E. Aldrian, "Characteristics of two mesoscale convective systems (MCSs) over the Greater Jakarta: case of heavy rainfall period 15–18 January 2013," *Geosci. Lett.*, vol. 6, no. 1, pp. 1–15, 2019, doi: 10.1186/s40562-019-0131-5.

[27] D. E. Nuryanto, "Keterkaitan Antara Monsun Indo-Australia Dengan Variabilitas Musiman Curah Hujan Di Benua Maritim Indonesia Secara Spasial Berbasis Hasil Analisis Data Satelit Trmm," *J. Meteorol. dan Geofis.*, vol. 13, no. 2, pp. 91–102, 2012, doi: 10.31172/jmg.v13i2.123.

[28] D. E. Nuryanto, R. Hidayat, H. Pawitan, and E. Aldrian, "The evolution of Mesoscale Convective System (MCS) around the Greater Jakarta area on 9 February 2015 using MTSAT Satellite," *Proc. - 39th Asian Conf. Remote Sens. Remote Sens. Enabling Prosper. ACRS 2018*, vol. 4, no. February 2015, pp. 2430–2438, 2018.

[29] D. E. Nuryanto, H. Pawitan, R. Hidayat, and E. Aldrian, "Kinematic and Thermodynamic Structures of Mesoscale Convective Systems During Heavy Rainfall in Greater Jakarta," *Makara J. Sci.*, vol. 22, no. 3, 2018, doi: 10.7454/mss.v22i3.8291.

[30] D. E. Nuryanto, H. Pawitan, R. Hidayat, and E. Aldrian, "The occurrence of the typical mesoscale convective system with a flood-producing storm in the wet season over the Greater Jakarta area," *Dyn. Atmos. Ocean.*, vol. 96, no. 2, p. 101246, 2021, doi: 10.1016/j.dynatmoce.2021.101246.

[31] T. Rigo and C. Farnell, "Quasi-Linear Convective Systems in Catalonia Detected Through Radar and Lightning Data," *Remote Sens.*, vol. 16, no. 22, 2024, doi: 10.3390/rs16224262.

[32] E. Tochimoto and H. Niino, "Tornadogenesis in a Quasi-Linear Convective System over Kanto Plain in Japan: A Numerical Case Study," *Mon. Weather Rev.*, vol. 150, no. 1, pp. 259–282, 2022, doi: 10.1175/MWR-D-20-0402.1.

[33] H. Chen, W. Xu, N. Liu, J. Sun, and J. Fu, "Climatologies of Mesoscale Convective Systems over China Observed by Spaceborne Radars," *Mon. Weather Rev.*, vol. 150, no. 10, pp. 2697–2717, 2022, doi: 10.1175/MWR-D-22-0002.1.

[34] S. Djakouré, J. Amouin, K. Y. Kouadio, and M. Kacou, "Mesoscale Convective Systems and Extreme Precipitation on the West African Coast Linked to Ocean–Atmosphere Conditions during the Monsoon Period in the Gulf of Guinea," *Atmosphere (Basel).*, vol. 15, no. 2, 2024, doi: 10.3390/atmos15020194.

[35] O. Ramos-Pérez, D. K. Adams, C. A. Ochoa-Moya, and A. I. Quintanar, "A Climatology of Mesoscale Convective Systems in Northwest Mexico during the North American Monsoon," *Atmosphere (Basel).*, vol. 13, no. 5, pp. 1–27, 2022, doi: 10.3390/atmos13050665.

[36] M. M. Wonsick, R. T. Pinker, and Y. Govaerts, "Cloud variability over the Indian monsoon region as observed from satellites," *J. Appl. Meteorol. Climatol.*, vol. 48, no. 9, pp. 1803–1821, 2009, doi: 10.1175/2009JAMC2027.1.

[37] H. Ismanto, "Karakteristik Kompleks Konvektif Skala Meso di Benua Maritim," *Tesis Inst. Teknol. Bandung*, 2011.

[38] M. A. Azka and N. J. Trilaksono, "COMPARATIVE ANALYSIS OF DIURNAL AND SEASONAL VARIATIONS IN PRECIPITATION OF MESOSCALE CONVECTIVE SYSTEM AND NON-MESOSCALE CONVECTIVE SYSTEM OVER," no. Mcc, pp. 83–92, 2025.

[39] E. Hermawan *et al.*, "Characteristics of Mesoscale Convective Systems and Their Impact on Heavy Rainfall in Indonesia's New Capital City, Nusantara, in March 2022," *Adv. Atmos. Sci.*, vol. 42, no. 2, pp. 342–356, 2025, doi: 10.1007/s00376-024-4102-1.

[40] V. Moron, A. Robertson, and J. Qian, "Multi-scale interactions during the Indonesian monsoon," May 2010.

[41] S. K. Dash, "Monsoons and monsoon climate," in *Encyclopedia of Earth Sciences Series*, J. E. Oliver, Ed., Dordrecht: Springer Netherlands, 2005, pp. 509–516. doi: 10.1007/1-4020-3266-8_142.

[42] J. Saroha, "Indian Monsoon : Origin and Mechanism," *Int. J. Res. Anal. Rev.*, vol. 4, no. 2, pp. 230–239, 2017.

[43] Y. Kajikawa, B. Wang, and J. Yang, "A multi-time scale Australian monsoon index," *Int. J. Climatol.*, vol. 30, no. 8, pp. 1114–1120, 2010, doi: 10.1002/joc.1955.

[44] M. A. Hasibuan and S. Amri, "[Research Article] Spatial Correlation between AUSMI and WNPMI Index with Rainfall in Jabodetabek," vol. 03, no. 1, 2025, doi: 10.69606/geography.v3i1.203.

[45] M. Dafri, S. Nurdiati, A. Sopaheluwakan, and P. Septiawan, "Analysis of climate indicator association with hotspots in Indonesia using heterogeneous correlation map," *IOP Conf. Ser. Earth Environ. Sci.*, vol. 893, no. 1, 2021, doi: 10.1088/1755-1315/893/1/012041.

[46] F. S. Pandia, B. Sasmito, and A. Sukmono, "Analisis Pengaruh Angin Monsun Terhadap Perubahan Curah

Hujan dengan Penginderan Jauh," *J. Geod. Undip*, vol. 8, no. 1, pp. 278–287, 2019.

[47] T. R. Syachputra, I. M. Radjawane, and R. Zuraida, "Kajian Statistik Ukuran Besar Butir Sedimen Dan Kaitannya Dengan Variabilitas Iklim Musiman Dan Tahunan Di Muara Gembong, Teluk Jakarta," *J. Ilmu dan Teknol. Kelaut. Trop.*, vol. 11, no. 3, pp. 683–695, 2019, doi: 10.29244/jitkt.v11i3.21961.

[48] A. Mulsandi *et al.*, "EVALUASI PERFORMA INDEKS MONSUN AUSMI DAN WNPMI DI WILAYAH INDONESIA Evaluation of WNPMI and AUSMI Monsoon Index Performance Over Indonesian Region," *J. Sains Teknol. Modif. Cuaca*, vol. 22, no. 2, pp. 61–70, 2021, [Online]. Available: http://www.cdc.noaa.gov/.

[49] L. M. V. Carvalho and C. Jones, "A satellite method to identify structural properties of mesoscale convective systems based on the maximum spatial correlation tracking technique (MASCOTTE)," *J. Appl. Meteorol.*, vol. 40, no. 10, pp. 1683–1701, 2001, doi: 10.1175/1520-0450(2001)040<1683:ASMTIS>2.0.CO;2.

[50] L. A. T. Machado, W. B. Rossow, R. L. Guedes, and A. W. Walker, "Life cycle variations of mesoscale convective systems over the Americas," *Mon. Weather Rev.*, vol. 126, no. 6, pp. 1630–1654, 1998, doi: 10.1175/1520-0493(1998)126<1630:LCVOMC>2.0.CO;2.

[51] J. Yuan and R. A. Houze, "Global variability of mesoscale convective system anvil structure from A-train satellite data," *J. Clim.*, vol. 23, no. 21, pp. 5864–5888, 2010, doi: 10.1175/2010JCLI3671.1.

[52] W. C. Chao and B. Chen, "The origin of monsoons," *J. Atmos. Sci.*, vol. 58, no. 22, pp. 3497–3507, 2001, doi: 10.1175/1520-0469(2001)058<3497:TOOM>2.0.CO;2.

[53] P. J. Webster, "The coupled monsoon system," *The Asian Monsoon*, no. 1987, pp. 3–66, 2006, doi: 10.1007/3-540-37722-0_1.

[54] Trismidianto and H. Satyawardhana, "Mesoscale Convective Complexes (MCCs) over the Indonesian Maritime Continent during the ENSO events," *IOP Conf. Ser. Earth Environ. Sci.*, vol. 149, no. 1, 2018, doi: 10.1088/1755-1315/149/1/012025.

[55] J. Yuan and R. A. Houze, "Deep convective systems observed by a-train in the tropical indo-pacific region affected by the MJO," *J. Atmos. Sci.*, vol. 70, no. 2, pp. 465–486, 2013, doi: 10.1175/JAS-D-12-057.1.

[56] C. M. Chu and Y. L. Lin, "Effects of orography on the generation and propagation of mesoscale convective systems in a two-dimensional conditionally unstable flow," *J. Atmos. Sci.*, vol. 57, no. 23, pp. 3817–3837, 2000, doi: 10.1175/1520-0469(2001)057<3817:EOOOTG>2.0.CO;2.

[57] S. Kouhen, B. A. Storer, H. Aluie, D. P. Marshall, and H. M. Christensen, "Convective and Orographic Origins of the Mesoscale Kinetic Energy Spectrum," *Geophys. Res. Lett.*, vol. 51, no. 21, 2024, doi: 10.1029/2024GL110804.